28th Symposium on Naval Hydrodynamics
Pasadena, California, 12-17 September 2010

Motion Prediction Using Wall-Resolved and Wall-Modeled Approaches on a Cartesian Grid

Jianming Yang, Thad Michael, Shanti Bhushan, Akira Hanaoka,
Zhaoyuan Wang, and Frederick Stern
(IIHR-Hydroscience & Engineering, University of Iowa,
Iowa City, IA 52242, USA)

ABSTRACT

CFDShip-Iowa version 6 is a high-fidelity, high-performance Cartesian grid solver for the multi-scale simulation of two-phase turbulent flows in ship hydrodynamics. In this paper, the recent development on motion prediction using wall-resolved and wall-modeled approaches is presented. First, a highly efficient, non-iterative, fully coupled scheme is developed for wall-resolved two-phase turbulent flows interacting with a solid body. In addition, an approximate domain approach is introduced for improved wall modeling using wall functions. Moreover, to develop more advanced wall models, an orthogonal curvilinear grid solver is coupled with the Cartesian grid solver using an overset grid methodology. Several other techniques, such as an efficient parallel fast marching method for wall distance calculation, a surface force calculation procedure for an immersed triangulated surface, and semi-Lagrangian advection schemes, are also developed. A series of validation cases including an elastically mounted circular cylinder in a free stream, the equilibrium state of square cylinder, laminar flows past a circular cylinder, and surface force for the Wigley hull, have been carried out. Results are compared with reference data to demonstrate the accuracy and applicability of the solver. Further development and enhancement is discussed.

INTRODUCTION

Simulation-based design for ship hydrodynamics requires simple and fast computation of hydrodynamic properties for numerous competitive hull geometries by design engineers who are not specialized in CFD (computational fluid dynamics) techniques. Tools based on potential flow theory have been applied to ship design for a long time. However, the lack of viscous effects and limited capacities for breaking waves in general potential flow solvers severely restrict their broader applications. The development of many RANS (Reynolds-averaged Navier-Stokes) solvers for viscous ship hydrodynamics over the last two decades and the recent dramatic increase in computing power has made the routine application of advanced RANS solvers in the ship design process possible. Nevertheless, traditional RANS solvers usually use data structures and algorithms that are not tailored for cost-effective computations on today's widely available commercial clusters and high-end tera- and peta-scale super-computers. Moreover, generating commonly used body-fitted structured grids is a highly sophisticated and time-consuming process. It requires a deep understanding of both the solver to be used and the flow field to be solved; this is a significant burden for a design engineer. These disadvantages greatly hinder wider application of these solvers in the ship design process.

Recently, considerable effort has been focused on developing approaches for simplifying or automating the grid generation process. The unstructured mesh methods and particle methods, e.g., SPH, are two very active fields working in this direction. However, the savings in grid generation are usually overwhelmed by penalties on accuracy and parallel performance due to the more complicated algorithms and data structures. On the other hand, Cartesian grid methods, which essentially eliminate the grid generation requirement, have also received increased attention and have been extended to viscous ship hydrodynamic applications in the last few years.

CFDShip-Iowa V6 is a Cartesian grid solver recently developed at IIHR for the high-performance, high-fidelity, multi-scale simulation of two-phase turbulent flows in ship hydrodynamics. It is based on a sharp interface immersed-boundary/level-set method for solid-liquid-gas systems and a Lagrangian dynamic subgrid-scale model for large-eddy simulations (LES). Some of its applications to the studies of bubble dynamics, wave-body interactions, and ship waves have been reported in Yang and Stern (2009). More

recently, an improved particle level set method (Wang et al., 2009a) and a coupled level set volume-of-fluid method with application to plunging breaking waves Wang et al., 2009b) were developed for enhanced two-phase interface capturing. One-equation Spalart-Allmaras and two-equation SST k-omega and k-g turbulence models with a wall function approximation for the immersed boundaries were implemented and applied to the DTMB model 5415 at Froude number 0.28 (Bhushan et al., 2010). Significant improvements for HPC (high-performance computing), such as three-dimensional domain decomposition, Hypre semi-coarsening multigrid Poisson solver, and parallel I/O using MPI2 were also accomplished (Yang et al., 2008b). At present, two concurrent efforts, one is coded V6.1 for immersed boundary approach with wall functions for wall modeling, the other is coded V6.2 for overset grid approach with orthogonal curvilinear boundary layer grid for wall modeling, are being performed to combine several enabling techniques into CFDShip-Iowa V6 for practical six DOF ship hydrodynamics applications.

One of the most important enabling techniques is the capability of predicting ship flows with six DOF motions on Cartesian grids. A strongly coupled scheme for fluid-structure interaction with multiple bodies was developed in Yang et al. (2008a) based on the direct forcing immersed boundary method in Yang and Balaras (2006). In this scheme, the fluid and the structure are treated as elements of a single dynamical system, and all the governing equations are integrated simultaneously and interactively in the time domain. As a predictor-corrector scheme, a few iterations between the fluid solver and the structure solver are involved. In each iteration, the positions of the immersed bodies will be changed and the relationship between the grid and the immersed boundaries has to be redefined; and the pressure Poisson equation has to be re-solved too. Therefore, an efficient setup procedure for the immersed boundaries is of importance. And the cost of the Poisson solver is critical. An alternative direct forcing immersed boundary approach for fluid-structure interactions given by Kim and Choi (2006) avoids the iterations in many strong coupling schemes by adopting a non-inertial reference frame. With such a frame fixed to the body, there is no relative motion between the body and the grid; the immersed boundary only needs to be set up once at the beginning of the simulation. More importantly, with an explicit, linear momentum forcing, a simple linear relationship between the fluid forces/moments acting on the body and the linear/angular velocities of the body was identified in Kim and Choi (2006), which enables a strongly coupled, direct update of the body velocities without iterations. In addition, the approach can effectively remove the wiggles in the forces and moments which exist in many immersed boundary methods due to the motions of immersed boundaries on the underlying fixed grid. In this study, the non-iterative strong coupling scheme in Kim and Choi (2006) has been implemented in CFDShip-Iowa V6 for the prediction of six DOF ship motion on a Cartesian grid.

An issue with the above linear reconstruction for the immersed boundary is that the whole interpolation stencil has to be within the viscous sublayer. For low and moderate Reynolds number turbulent flows, this wall-resolved approach is usually feasible considering the current widely available HPC power. However, for high Reynolds number flows, the wall-resolved approach imposes prohibitive grid resolution requirements, even for solvers using body-fitted grids. Therefore, wall-modeled approaches have to be adopted to enable the solver to be used in practical engineering applications.

There are three broad classes of wall models: (1) bypassing the near-wall region all together using wall-functions, (2) zonal approach, where linearized Navier-Stokes equation are solved on lower-dimensional grids embedded between the first grid point and the wall using outer grid results as boundary condition, and (3) hybrid RANS/LES approach, where RANS equations are solved in the near-wall region and LES in the outer region. Hybrid RANS/LES can be used for a single grid where the solver is modified via turbulence modeling or hybrid grids which allow use of different solvers suited in RANS and LES regions.

Wall modeling using a multi-layer wall-function approach for CFDShip-Iowa V6 was tested in a straightforward manner in Bhushan et al. (2010). Simulations for a ship model DTMB 5415 in the straight ahead condition with y^+=30 showed that the wall functions as implemented have limitations in accurately predicting flow separation and turbulence quantities. A major concern with the wall function implementation in Bhushan et al. (2010) is the irregular behavior of pressure near the immersed boundary due to the coupled pressure solution and the velocity jump across the immersed boundary from the non-linear wall function approximation. To decouple the pressure solution, an approach similar to the approximate domain method developed in Kang et al. (2009) has been implemented to remove the region occupied by the solid phase and impose the pressure boundary condition at the immersed boundary.

Wall functions are more suited to body fitted grids for which uniform first grid point spacing can be maintained over the hull surface, whereas on a Cartesian grid an embedded body-fitted grid has to be

used to realize the same property. Therefore, an alternative approach is to use a body fitted curvilinear grid to resolve the boundary layer and a Cartesian grid elsewhere. The Chimera or overset grid methodology (Carrica et al., 2008) allows the construction of complex multi-body configurations from sets of relatively simple overlapping grids using appropriate inter-grid communication. This approach is applicable for finite difference solvers and has been previously used for ship hydrodynamics applications by the authors. In this study, a body fitted orthogonal curvilinear grid solver (Suh et al., 2010), which is extended from Yang and Stern (2009) and has the same software architecture, is coupled with the Cartesian grid solver using the overset approach. The overset grid approach provides a framework for interpolating variables between the background and wall layer grids, and can be applied to velocity and turbulence variables in a straightforward fashion. For the Cartesian grids the interpolated grid (fringe) points are treated similar to the forcing points in the immersed boundary methods, whereas the fringe points for the boundary layer grid act as boundary conditions. To satisfy mass conservation across the overset grid, the pressure Poisson equation is solved in a strongly coupled manner using the PETSc toolkit (Balay et al., 1997).

Several other enabling techniques have also been developed. One of them is an efficient parallel fast marching method for distance function calculation. The wall distance function is usually required in RANS and DES (detached eddy simulation) models. Also, in the immersed boundary methods, the introduction of a body level set function can simplify many tasks for identifying the body-grid relationship. However, the calculation of wall distance functions is not simple in a parallel environment. In general, brute force approaches are inefficient and non-scalable. The iterative approaches like the level set reinitialization equation, which solves the Eikonal equation using high-order schemes, are expensive. The fast marching method by Sethian (1996) is very efficient, but the original algorithm is serial. Herrmann (2003) reported the first domain decomposition parallelization of the fast marching method, but his method is not very efficient because of a complicated communication model. We developed a simple and efficient algorithm for the parallel implementation of the fast marching method. Some data from this method will be presented in the Results section to demonstrate its efficiency.

Another technique is the surface force calculation from the surface triangulation in the immersed boundary method. Without a body-fitted grid, the calculation of the pressure and shear on the hull is not straight forward. Because the pressure and shear on the hull are not known from a body-fitted grid, they must be extrapolated from the Cartesian grid. For a linear reconstruction, the extrapolation is relatively easy. However, with a wall function reconstruction, the points from which the information is extracted have to be chosen very careful to produce realistic results. Several strategies will be discussed in this study.

In addition, semi-Lagrangian advection schemes are implemented in the Cartesian grid solver to address the issue of very tight time step constraints due to the explicit treatment of the Eulerian convection terms in some multi-scale simulations. The violent interface topological evolution may severely restrict the time step due to the CFL condition. Compared to the fully implicit schemes, which result in non-symmetric linear systems and require iterative solvers for the equations, the semi-Lagrangian schemes have several advantages. They are unconditionally stable and can significantly improve the CFL condition, i.e., by one order of magnitude without involving non-symmetric linear systems. A direction-splitting semi-Lagrangian volume of fluid method for interface capturing has also been developed. The geometric properties such as normal and curvature are evaluated using the volume fraction itself instead of the level set function. Using this method, the level set advection step is avoided, which represents a significant computational savings, and the level set is obtained from a redistancing step using the volume fraction field.

COMPUTATIONAL METHODS

For simplicity, vector notation will be used for all equations without regard to the coordinate systems in the following sections unless stated otherwise. The governing equations and discretizations in indicial notation for orthogonal curvilinear coordinates were given in Yang et al. (2008b).

Mathematical Modeling

Navier-Stokes Equations

Incompressible viscous flows of two immiscible fluids, e.g., air and water, are governed by the Navier-Stokes equations:

$$\frac{\partial \mathbf{u}}{\partial t} + \mathbf{u} \cdot \nabla \mathbf{u} = \frac{1}{\rho} \nabla \cdot \left(-p\mathbf{I} + \mathbf{T} \right) + \mathbf{g} , \tag{1}$$

$$\nabla \cdot \mathbf{u} = 0 , \tag{2}$$

where t is the time, $\mathbf{u}$ is the velocity vector, p is the pressure, $\boldsymbol{I}$ is the unit diagonal tensor, ρ is the density, $\mathbf{g}$ represents the gravity acceleration, and $\mathbf{T}$ is the viscous stress tensor defined as

$$\mathbf{T} = 2\mu \mathbf{S} , \tag{3}$$

with μ the dynamic viscosity and **S** the strain rate

$$\mathbf{S} = \frac{1}{2}\left(\nabla\mathbf{u} + (\nabla\mathbf{u})^T\right). \quad (4)$$

Turbulence Modeling

Equations (1-2) can be spatially filtered (LES) or temporally averaged (RANS) to reduce the direct numerical simulation (DNS) resolution requirements at the price of turbulence closure problems for LES or RANS. The subgrid-scale stress tensor or the Reynolds stress tensor from these operations can be parametrized following Smagorinsky's procedure for the LES approach or Boussinesq's hypothesis for the RANS approach. Therefore, the momentum equation can be rewritten in the following form

$$\frac{\partial\bar{\mathbf{u}}}{\partial t} + \bar{\mathbf{u}}\cdot\nabla\bar{\mathbf{u}} = -\frac{1}{\rho}\nabla\bar{p} + \nabla\cdot\left[\nu_t\left(\nabla\bar{\mathbf{u}} + (\nabla\bar{\mathbf{u}})^T\right)\right] + \frac{1}{\rho}\nabla\cdot\left[\mu\left(\nabla\bar{\mathbf{u}} + (\nabla\bar{\mathbf{u}})^T\right)\right] + \mathbf{g} \quad (5)$$

Where ν_t is the turbulent eddy viscosity, which can be obtained from a Lagrangian dynamic Smagorinsky subgrid-scale model (Meneveau et al., 1996) for LES or from solving the turbulence model equations, such as the Spalart and Allmaras (1992) model, the SST k-omega model (Menter, 1994), and the k-g model (Kalitzin et al., 2005).

Interface Modeling

Defining the interface Γ as the zero level set of a signed distance function, ϕ, or the level set function, the position of the interface can be tracked by solving the level set evolution equation

$$\frac{\partial\phi}{\partial t} + \mathbf{u}\cdot\nabla\phi = 0. \quad (6)$$

To keep the level set function as a signed distance function in the course of the evolution, we iterate the reinitialization equation for the level set function (Sussman et al., 1994).

In the coupled level set volume-of-fluid method, the volume-of-fluid function, *F*, is defined as the liquid volume fraction in a cell with its value in between zero and one in a surface cell and zero and one in air and liquid respectively. The advection equation of *F* is

$$\frac{\partial F}{\partial t} + \mathbf{u}\cdot\nabla F = 0\cdot \quad (7)$$

With the level set function defined, the fluid properties, such as density and viscosity, are given by the following equations:

$$\rho = \rho_G + (\rho_L - \rho_G)H(\phi), \quad \mu = \mu_G + (\mu_L - \mu_G)H_\varepsilon(\phi), \quad (8)$$

where the subscripts *G* and *L* represent gas and liquid phase, respectively. In this paper, the density keeps a sharp jump, whereas the viscosity is smoothed over a transition region across the interface using the smoothed Heaviside function (Sussman et al., 1994).

Numerical Method

Two-Phase Flow Solver

The finite differences method is used to discretize the Navier-Stokes equations on a non-uniform staggered Cartesian grid (and an orthogonal curvilinear grid for V6.2), in which the velocity components *u*, *v*, and *w* are defined at centers of cell faces in the *x*, *y*, and *z* directions, respectively, and all other variables, i.e., *p*, ϕ, ρ, μ, and ν_t are defined at cell centers. An explicit time-advancement scheme is adopted to integrate the momentum equations with the second-order Adams-Bashforth scheme. A fractional-step method is employed for velocity-pressure coupling, in which a Poisson equation is solved to enforce the continuity equation. In the momentum equation, the convective terms are discretized using a third-order QUICK scheme (Leonard, 1979) and higher-order WENO schemes (Jiang and Shu, 1996) are available. All other terms are discretized with the standard second-order central difference scheme. The parallelization is done via a domain decomposition technique using the MPI library. The Poisson equation is solved using the PETSc library (Balay et al., 1997) or a semi-coarsening multigrid Poisson solver from the Hypre library from Lawrence Livermore National Laboratory (Falgout et al., 2006). In general, the Poisson solver is the most expensive part of the whole algorithm.

Non-Iterative Strong Coupling Scheme for Fluid-Structure Interactions

For fluid-structure interaction problems, the non-iterative strong coupling scheme in Kim and Choi (2006) is extended to the liquid-solid-gas system in ship hydrodynamics. A non-inertial reference frame is used. In this study, the rotation matrix for the conversion between the inertial and non-inertial reference frames reduces to an identity matrix and the angular velocity vector due to the coordinate transformation becomes zero. The governing equations become the same as those for a moving grid system in an inertial reference frame. That is, in the advection terms, the grid moving velocity vector (body velocity) is subtracted from the advecting velocity vector.

In the current direct forcing immersed boundary method, the effects of the immersed bodies are fully

represented by the extra forcing term added to the momentum equation. Therefore, for these approaches, a straightforward way of evaluating the forces and moments is to perform an integration of the forcing term pointwise. Actually, the method in Kim and Choi (2006) was built on top of this concept. The momentum forcing term has a direct dependence on the velocity of the rigid body. For a strong coupling scheme, the forces and moments at current time step are required to solve the dynamic equation for rigid body motion to obtain the current body velocity. An exclusive advantage from the non-inertial reference frame, or, a body-fixed grid, is the prediction of position/orientation of the rigid body at the current time step becomes unnecessary. More importantly, as shown by Kim and Choi (2006), if a provisional step of using the body velocity of previous time step to evaluate the forcing term is taken, then there exists a linear relationship between the difference of these two forcing terms (the current and the provisional) and the body velocity vector increment: If this relationship is used in the discretized equations for rigid body dynamics, these equations can be solved implicitly without iterations, which is highly desirable due to the very expensive step of solving the Poisson equation. The details of the whole algorithm were given in Yang and Stern (2010).

Immersed Boundary Approximate Domain Method

In the direct forcing immersed boundary methods, the flow field is solved everywhere, including inside of any bodies. In the immersed boundary approximate domain method (IBADM) by Kang et al. (2009), only the regions of the flow field that are not intersected by or enclosed by the body are solved, as shown in Fig. 1. This solution domain requires special treatment of the boundary conditions near the body. The approximate domain method was introduced in Kang et al. (2009) for an unstructured, finite volume method on a node-based collocated grid. The present work applies a similar idea for a structured, finite difference method on a staggered grid.

Creating new domain boundaries prevents the use of cells with non-physical velocities, and therefore non-physical divergences, from being used in the pressure solver. Because the new approximate domain is not body fitted, non-zero velocities must be specified at the boundaries. These velocities are determined using the local flow field and velocity of the body. Wall functions may be used, which is important for ships which tend to operate at very high Reynolds numbers.

One of the weaknesses of the original immersed boundary treatment in V6-IBM (Yang and Stern, 2009) is that continuity is not enforced at the body surface at all. The IBADM seeks to improve this by enforcing continuity around the body in a global sense. The boundary velocities are integrated to find a net boundary flux. Correction factors are then applied to force the net boundary flux for each body to zero. On a staggered mesh, to avoid large differences in corrections to cells with inflow on one side and outflow on another side, the application of the correction factors is based on the total flux for each cell rather than the flux through each face.

In the first step of this approach, a list of intersected cells is constructed during initialization. Separate lists are maintained for each body so that if a body moves its list can be updated without disturbing the other lists. The list of intersected cells is used to build a list of boundary cells for the approximate domain. The list of boundary cells is then used to build a list of points requiring velocity specification and whether they lie on the boundary or not. Velocities also need to be specified at points adjacent to the boundary to create the viscous boundary layer. The points adjacent to the boundary may be in boundary cells or in the intersected cells as shown in Fig. 1.

After the convection step, the velocities are specified at points on the list using wall functions or linear interpolation between points in the approximate domain and the closest point on the body.

Before solving the pressure Poisson equation, solid and intersected cells are deactivated by setting the right-hand side and off-diagonal matrix terms to zero while setting the matrix diagonal terms to one for those cells. This method is compatible with the Hypre geometric and algebraic multigrid solvers (Falgout et al., 2006).

The pressure derivatives are set to zero at the boundary cells to prevent the subsequent alteration of the boundary velocities during the corrector step.

Coupled Cartesian/Curvilinear Grid solver

In the coupled curvilinear/Cartesian grid solver (V6.2) both V6-IBM and V6-OC solvers run simultaneously on separate MPI communicators, velocities and turbulence quantities are interpolated, and the coupled pressure Poisson equation is solved to satisfy mass conservation. The flow chart in Fig. 2 demonstrates the solver structure.

The overset grid information is obtained using SUGGAR (Noack, 2006) using the cell centered grids for both the solvers as shown in Fig. 2. SUGGAR currently supports a structure grid function which allows the two outermost (JMAX and JMAX-1, herein) planes of the wall-layer grid to be fringe points. The overset grid information file is generated beforehand

for the static grids and read as an input file. The file provides the information regarding the fringe points and their donors, and the hole points in the Cartesian grids which are excluded from the solution. For dynamic grids, the SUGGAR libraries can be called each time step to update the overset grid information.

The velocity and turbulence interpolation in V6-IBM is similar to the IBM boundary condition specification, and is specified as dirichlet boundary conditions for V6-OC. For the velocity interpolation, the contravariant velocities in V6-OC are first transformed to Cartesian components, and then interpolated at cell centers. The updated velocities at the fringe point for V6-OC are transformed back to the contravariant components. The values at the staggered grid are obtained using tri-linear interpolation using the surrounding fluid and fringe points for both the solvers. The cell center interpolation of the scalar turbulence quantities do not require transformation or staggered grid interpolation.

The coupled pressure Poisson equation is solved using PETSc for which the MPI communicator encompasses processors from both the solvers. The left hand side (LHS) matrix consists of a 7-point stencil for the fluids points, 9-point stencil for the fringe points, and 1-point stencil for the hole points. The LHS matrix is assembled only at the first time step as grids are static, and the right hand side (RHS) vector is updated every time step. The pressure Poisson equation for the fluid points is:

$$\nabla \cdot \left(\frac{1}{\rho} \nabla p \right) = -\frac{1}{\Delta t} \nabla \cdot \mathbf{u}^* \tag{9}$$

For an internal grid point, the discretization of this equation using a standard seven-point stencil becomes:

$$\begin{aligned} &C_{i,j,k-1} p_{i,j,k-1} + C_{i,j-1,k} p_{i,j-1,k} + \\ &C_{i-1,j,k} p_{i-1,j,k} + C_{i,j,k} p_{i,j,k} + \\ &C_{i+1,j,k} p_{i+1,j,k} + C_{i,j+1,k} p_{i,j+1,k} + \\ &C_{i,j,k+1} p_{i,j,k+1} = RHS_{i,j,k} \end{aligned} \tag{10}$$

where the diagonal component of the LHS matrix is

$$\begin{aligned} C_{i,j,k} = &-C_{i,j,k-1} - C_{i,j-1,k} - C_{i-1,j,k} \\ &-C_{i+1,j,k} - C_{i,j+1,k} - C_{i,j,k+1} \end{aligned}. \tag{11}$$

For points next to a physical boundary, Neumann boundary condition is applied. The pressure is interpolated for the fringe points:

$$p_{i,j,k} - \sum_{m=1}^{8} w_m p_m^d = 0, \tag{12}$$

where i,j,k is the fringe point index, P_m^d is the pressure for a donor point, and W_m is the corresponding interpolation weighting factor. For the hole points:

$$p_{i,j,k} = 0. \tag{13}$$

The LHS and RHS matrices are assembled as a single linear system, which is solved using Krylov subspace based GMRES iterative method with ASM preconditioner.

Thus far single phase equations are solved using a dynamic Smagorinsky model for LES. The numerical approach is the same as that of the Cartesian and curvilinear grid solvers, except the discretization of the convective terms, which is reduced to the 3rd order QUICK scheme for the orthogonal curvilinear solver. The order of convection term is reduced because the overset interpolation is obtained only for 2 J-planes, whereas 5th order discretization requires interpolation for 3 J-planes. The velocity interpolation is performed after the predictor, first and second corrector steps. The subgrid-scale eddy viscosity is updated only once after solving the dynamic Smagonisky model after the second corrector.

Efficient Parallel Fast Marching Method for Wall Distance Calculation

The fast marching method (Sethian, 1996) is a widely used numerical method for solving the Eikonal (static Hamilton-Jacobi) equation

$$\left| \nabla \phi \right| = 1, \tag{14}$$

which is a first-order hyperbolic partial differential equation. The fast marching method has theoretically optimal complexity in its operation count by exploring the causality of the Eikonal equation and adapting a one-pass updating strategy. The Eikonal equation describes nonlinear boundary value problems in which the information from the boundary propagates away along characteristics. In the fast marching method, upwind difference schemes are used to discretize the Eikonal equation at a given grid point, such that the stencil contains only neighboring points with valid values (or, upwind points) and the causality of the equation is strictly followed. Moreover, a heap priority queue is used to march the solution in a rigorous increasing (decreasing for negative solution) order. Therefore, the number of times that a point is visited is minimized and no iterations are involved in the whole process. Since the run-time complexity of reordering of a heap of length n is O(log n), the fast marching method has a total operation count of O(N log N) for a case involving N grid points.

The first attempt to parallelize the fast marching method based on domain decomposition technique was reported by Herrmann (2003). In his approach, the computational domain is decomposed into non-overlapping grid blocks and ghost nodes (one layer for a first-order scheme) are used for inter-block communication. The serial fast marching algorithm is practically executed in each block with the addition of several elements accounting for the parallelization. For the ghost node communication, if a just-accepted node belongs to the ghost domain of a neighboring block, then the information of this node will be sent to the target neighbor. In the mean time, each process repetitively checks for updated ghost nodes from its neighbors; a rollback mechanism is introduced to revoke the valid status of all pre-accepted nodes whenever a ghost node turned to valid status with a smaller value than these nodes. A process that reaches the end of the serial algorithm (empty heap or narrow band exceeded) has to wait for all other processes scoring the same status; also, it has to check for ghost node updates from neighbors and re-initiate the whole algorithm when a rollback operation is triggered. The asynchronous communications in this algorithm, especially for terminating the whole computation, are quite involved and difficult to implement. The rollback operation incurs significant communication and computation overhead and considerably limits the parallel efficiency. Moreover, only a first-order scheme was implemented in Herrmann (2003). The use of high-order schemes could further deteriorate the efficiency due to the increased rollback operations from two or more layers of ghost nodes.

In this study, we developed an algorithm that can achieve higher speed-up and is simpler to implement. With the same test by Herrmann (2003), nearly linear speedup was observed up to 64 processors and super-linear speedup was achieved for optimal domain decomposition.

Force Calculation on an Immersed Triangulation

Prediction of ship resistance and motions are the most common uses of CFD for ships. Without a body-fitted grid, the calculation of the pressure and shear on the hull is not straight forward. Because the pressure and shear on the hull are not known from a body-fitted grid, they must be interpolated from the Cartesian grid. Different strategies can be applied to pressure and shear stresses.

In the case of pressure, the standard boundary layer assumption that pressure is constant normal to the wall can be employed. However, it is important to pay attention to computing the local normal vector. When the body is represented as a triangulated surface and the stagnation point is on a sharp edge, the normal vectors of the facets will not point forward and the stagnation pressure will not be captured. To capture the stagnation point at a sharp edge, the average normal vector at each vertex is computed using an area-weighted average of normal vectors of the facets sharing that vertex.

In the case of shear stress, both laminar flow and wall functions must be considered. Wall functions are typically required for the high Reynolds numbers that occur in ship flows. In either case, the velocity tangent to the surface at some distance from the hull must be determined. That distance must be selected so that the interpolation will not involve points inside of the body, or, in the case of the approximate domain method, points outside of the approximate domain. Simultaneously, the distance should not be further from the body than required. This is accomplished by computing the local cell size in the direction of the normal vector.

Once the pressure and shear stresses at the hull vertices have been computed, force and moment integration is performed. The integration of forces on the hull could be performed using the triangulation of the body supplied to the CFD code. However, if the facets are larger than the CFD grid, resolution and accuracy may be reduced. To overcome this limitation, facets on the body are compared with the local cell size and subdivided when required. In this way, the resolution of the flow solution is maintained in the case of a coarse body surface triangulation.

Semi-Lagrangian Advection Schemes

In the explicit Eulerian advection schemes, the maximum time step is subject to the CFL number, which leads to a prohibitive time step restriction for the advection-dominated problems. Implicit advection schemes can relax the time step constraints from the CFL condition, but need Newton iterations and non-symmetric solvers. On the other hand, semi-Lagrangian treatment of the advection terms can significantly increase the maximum allowable time step with CFL number up to 4-5; and it is unconditionally stable. It also produces a symmetric matrix and maintains the efficiency of symmetric solvers.

Two steps are involved in the semi-Lagrangian schemes, the backward integration and interpolation. In the backward integration, the departure point of a fluid particle arriving at a grid point is located. The departure point usually does not coincide with a grid point. Therefore, the solution value needs to be interpolated at the departure point. Tri-linear or higher-order (e.g., ENO) schemes can be used for interpolation.

In this study, a direction splitting semi-Lagrangian volume-of-fluid method is developed. Also, a semi-

Lagrangian scheme for the Navier-Stokes equations has been implemented.

RESULTS

Fluid-Structure Interaction on a Cartesian Grid

Two DOF Oscillating Circular Cylinder

The non-dimensionalized dynamic equation for an elastically mounted body can be written as follows:

$$\ddot{\mathbf{x}} + 2\zeta\left(\frac{2\pi}{U^*}\right)\dot{\mathbf{x}} + \left(\frac{2\pi}{U^*}\right)^2 \mathbf{x} = \frac{4}{\pi m^*}\mathbf{f}, \qquad (15)$$

where **x** is the displacement of the body in (x,y) plane nondimensionalized by the length scale *D* (cylinder diameter here), the reduced velocity is defined as $U^* = U_\infty / (f_N D)$ with the freestream velocity U_∞ and the natural vibration frequency of the structure $f_N = (1/2\pi)\sqrt{k/m}$, and the mass ratio between the structure and the fluid is defined as $m^* = m/m_f = m/(\rho_f \pi D^2/4)$ with m_f mf the mass of the fluid replaced by the structure and ρ_f the fluid density, $\zeta = c/\sqrt{4km}$ is the damping ratio, and **f** is the hydrodynamic force vector (f_x, f_y) normalized using $\rho_f D U_\infty^2$. In the above, *m* is system mass, *c* the damping coefficient, *k* the spring constant.

A circular cylinder oscillating in the (x; y) plane was considered. The Reynolds number was set to Re = 200, the reduced velocity was U* = 5.0, and the damping ratio was ζ = 0.01. The mass ratio was set to be $4/\pi$. The computational domain is [-10D, 30D] in the streamwise direction and [-10D, 10D] in the transverse direction, respectively. At the inflow boundary a uniform velocity was specified. At the outflow boundary a convective boundary condition was used. Neumann boundary conditions were applied at the top and bottom boundaries. The number of grid points was 400×360 in the streamwise and transverse directions respectively, with a resolution of approximately 0.02D×0.02D near the cylinder.

The corresponding stationary cylinder problem was first solved and then free vibrations in both directions were allowed. Due to the low mass ratio in this case, a stable periodic state was achieved much faster compared to the previous problem. This case was given by Blackburn and Karniadakis (1993) using a higher-order spectral element method with an accelerating reference frame. In Yang et al. (2008a) a 4th-order predictor-corrector strong coupling scheme was applied to this case too. The predicted trajectory of the cylinder center during the periodic steady state is shown in Fig. 3. Our current results from the non-inertial reference frame agree very well with the spectral simulation and the inertial reference frame simulation. In the latter, however, the origin is slightly shifted downstream by 0:0185D due to a 3% difference in drag force, which is reasonable because surface force integration was used in the latter and usually the shear stress was estimated a little lower than the actual value as a result of linear extrapolation in the surface force calculation. The displacements in both directions are also shown in Fig. 4 as functions of time. The time evolution of the drag and lift forces is shown in Fig. 5, which is in good agreement with the reference results. In Fig. 6, a snapshot of vorticity shedding from the cylinder is shown for an instant in time during the periodic steady state. The vortex pattern in the wake resembles the one that has been observed in Yang et al. (2008a).

Equilibrium State of a Floating Square Cylinder

In this case, a half-buoyant square cylinder of side length D=2m was held still with the center 0.5m below the free surface. It was released at time t = 0s. According to Archimedes' law, the cylinder reached its equilibrium state, in which half of the cylinder was above the free surface, after some time. The buoyancy force at the final equilibrium state should be $0.5D^2L\rho_{water}$ g, which is 19.6kN for a cylinder of length L = 1m.

A grid of 200×120 was used in this simulation with local grid spacing of 0.02D around the cylinder. Since a non-reflecting boundary condition was not applied in this study, the simulation took a long time to reach the equilibrium state. Fig. 7 shows the free surface profiles at several instances, e.g., the initial state of 3/4 portion submerged and the final state of 1/2 portion submerged.

Figure 8 shows the time history of the vertical force on the cylinder, after a long time, the equilibrium force 19.6kN is reached. The corresponding time history of the vertical velocity of the cylinder is shown in Fig. 9 and the approaching to a zero velocity is illustrated.

Immersed Boundary Approximate Domain Simulation of Laminar Flow past a Cylinder at Re=200

This vortex shedding cylinder case was computed on a 180×244 non-uniform grid and compared with results from Xu (2008). The drag and lift coefficients are shown in Table 1. Fig. 10 compares the computational results from the IBADM with the IBM, overset (V6.2), and data from Xu (2008). The results from IBADM agree well with other reference data.

Overset Boundary Layer Grid Simulation of Laminar Flow past a Cylinder at Re=200

The computational domain is X = [-20, 20] and Y = [-11,11]. For V6-IBM, it is discretized using 204×260 points in X and Y directions, respectively. The V6.2 domain size and background grid is same as that of V6-IBM. The boundary layer grid of thickness $0.2D_o$ is 22×128 in the radial and azimuthal directions, respectively. The overset grid configuration is shown in Fig. 11.

For V6-IBM uniform inlet and convective boundary conditions are specified at I-MIN and I-MAX planes, respectively. Slip wall conditions are specified at rest of the boundaries, and IBM approach is used for the wall boundary condition. For V6.2, background Cartesian grid is used to specify inlet, exit and slip walls boundary condition away from the wall, and WL J-MIN plane specifies the no-slip boundary condition. The WL and background solvers communicate via the overset boundary conditions.

An unsteady vortex shedding is predicted by all the solvers, as shown in Fig. 12 for V6.2 predictions. As shown in Table 1, *St* of the shedding compares within 1% between the code and those reported by Xu (2008) and averaged CFD results surveyed therein. Mean C_d is predicted within 3% of the benchmark CFD results for V6-IBM, but C_d and C_l amplitudes are under predicted by 6% as shown in Fig. 10. Mean C_d prediction is 5% lower for V6.2. However, the amplitude is predicted within 3% for V6.2.

Parallel Fast Marching Method

In this test, a cubic domain is used and the interface is a sphere of diameter 0.5, which is located at the center of the domain $\mathbf{x}_c$ = (0.5; 0.5; 0.5). The signed distance function can be given by $\phi = 0.25 - |\mathbf{x} - \mathbf{x}_c|$. A uniform grid of 192×192×192 is used to discretize the domain. Fig. 13 shows the interface and contours lines in a center slice of the volume.

Figure 14 shows the parallel speedup of the current method in this test. Very good scalability was observed up to 512 processors. Linear speedup was obtained up to 64 processors. Especially, with optimal domain decomposition, super-linear speedup was achieved.

Figure 15 shows an example of the signed distance function for the Wigley hull.

Surface Force Calculation

The Wigley hull has been computed using the immersed boundary method with wall functions (Bhushan et al., 2010). The selected conditions correspond to a Froude Number of 0.267 and Reynolds Number of 2.2×10^6. A grid with 14.5 million cells was used, with an average y+ of 75. Fig. 16 shows the pressure distribution on the body determined by interpolation from the flow field at points normal to the hull compared with results from the body-fitted code CFDShip-Iowa version 4 (Huang et al., 2007). The computed drag coefficient is 11 percent less than measured (D'Este and Contento, 2003).

Semi-Lagrangian Advection Schemes

Figure 17 shows the case of lid-driven cavity flow using both the Eulerian and semi-Lagrangian advection schemes. A CFL number of 20 for the latter can still produce very similar results to the former with a CFL of 0.6. Fig. 18 shows the advection test of a single vortex flow and it is evident that the current semi-Lagrangian scheme can retain the same accuracy as the Eulerian scheme, but with much larger time steps.

CONCLUSIONS AND FUTURE WORK

In this paper, recent developments for ship motion prediction using wall-resolved and wall-modeled approaches in CFDShip-Iowa V6 have been presented. Progress on various fronts has been demonstrated and discussed. First, a very efficient non-iterative strong coupling scheme for fluid-structure interactions in the liquid-solid-gas system has been developed. Second, an immersed boundary approximate domain method for decoupling pressure across the immersed boundary has been implemented. Wall function approaches based on this method are currently under development. Third, an overset grid method using an orthogonal boundary layer grid as a new wall modeling strategy on a Cartesian grid has been investigated and promising results have been observed. Several other key enabling techniques, such as a parallel fast marching method for efficient wall distance calculation, a surface force calculation procedure for immersed triangulations, and semi-Lagrangian advection schemes, have been implemented in V6.1. Various test cases have been performed and compared with reference data. Satisfactory agreement has been observed.

In terms of future work for V6.1, the wall-resolved approach using non-iterative strong coupling scheme will first be validated with simulations involving large angle rotation. Then it will be applied to predict ship motion such as dynamic sinkage and trim and pitch and heave in regular waves using grids of billions of points. The high resolution is very feasible as in the current scheme the Poisson equation is solved only once and the computational cost is considerably lower than the scheme that iteratively solves the strongly coupled fluid-structure interaction problems. The wall functions in V6.1 will be refined by combining it with the newly

implemented approximate domain approach. The non-iterative scheme cannot be directly applied for this approach as the local reconstruction for imposing wall boundary conditions at the immersed boundary is not linear any more. Therefore, the predictor-corrector scheme in Yang et al. (2008a) will be applied for the wall-modeled motion prediction using wall functions in V6.1. In each iteration, the position of the immersed body (ship) will be changed. Thus the immersed boundary treatment has to be set up repeatedly in each time step. A very efficient one-pass setup procedure for immersed boundary treatment is currently being tested. With this new setup procedure, the element in the surface triangulation will be visited only once for a new position of the body. For a high resolution surface triangulation on a grid of hundreds of millions of points, the new procedure can save a significant portion of the total computational cost. The new algorithms, i.e., the parallel fast marching method, surface force calculation procedure, and the semi-Lagrangian advection schemes, will be combined into V6.1 for even more desirable efficiency.

Future validation for V6.2 will focused on moderate and high Reynolds single and two phase flows. Currently validation for single phase turbulent flow Re = 3900 over a circular cylinder using LES is in progress. Benchmark results using orthogonal results have been obtained which shows good agreement with the EFD, and simulations using the wall-layer Cartesian grid solver are in progress. The circular cylinder validation study will be extended for $Re = 5\times10^5$. Following that, interface modeling subroutines will be coupled and validated for a surface piercing circular cylinder at $Re = 2.7\times10^4$, $Fr = 0.4$ for which benchmark orthogonal curvilinear solver results are already available (Suh et al., 2010). The wall-layer model will be applied to the Wigley hull with fixed sinkage and trim at Re=2.2×10^6, Fr=0.267, and the limitations of the orthogonal grid assumption will be evaluated.

ACKNOWLEDGMENTS

This research was sponsored by the Office of Naval Research under Grant N00014-01-1-0073 and N00014-06-1-0420, under the administration of Dr. Patrick Purtell. The authors would also like to thank Dr. Pablo Carrica for his valuable suggestions and help with the overset grid technique.

REFERENCES

Balay, S., Gropp, W.D., McInnes, L.C. and Smith, B.F., "Efficient Management of Parallelism in Object Oriented Numerical Software Libraries," in Modern Software Tools in Scientific Computing, Edited by E. Arge, A.M. Bruaset and H.P. Langtangen, Birkhäuser Press, 1997, pp. 163–202.

Bhushan, S., Carrica, P.M., Yang, J. and Stern, F., "Scalability Study and Large Grid Computations for Surface Combatant Using Cfdship-Iowa," International Journal of High Performance Computing, 2010, under revision.

Blackburn, H.M. and Karniadakis, G.E., "Two- and Three-Dimensional Simulations of Vortex-Induced Vibration of a Circular Cylinder," Proceedings of the Third International Offshore and Polar Engineering Conference, Singapore, 1993, pp. 715-720.

Carrica, P. M., Wilson, R. V., Noack, R. W. and Stern, F., "Ship Motions Using Single-Phase Level Set with Dynamic Overset Grids," Comput. Fluids, Vol. 36, 2007, pp 1415-1433.

D'Este, F. and Contento, G., "Time Domain Linear and Weakly Nonlinear Coupled Wave Resistance and Seakeeping Computations," Science and Supercomputing at CINECA, Report, 2003.

Falgout, R. D., Jones, J. E. and Yang, U. M. "The Design and Implementation of HYPRE, Library of Parallel High Performance Preconditioners," Numerical Solution of Partial Differential Equations on Parallel Computers. A.M. Bruaset and A. Tveito, eds. Springer-Verlag. Vol. 51, 2006, pp. 267-294.

Herrmann, M., "A Domain Decomposition Parallelization of the Fast Marching Method," Annual Research Briefs-2003, Center for Turbulence Research, Stanford, CA, 2003, pp. 213–226.

Huang, J., Carrica, P. M. and Stern, F. "Coupled Ghost Fluid/Two-Phase Level Set Method for Curvilinear Body Fitted Grids," Int. J. Num. Meth. Fluids, Vol. 55, 2007, pp. 867-897.

Jiang, G.-S. and Shu, C.-W., "Efficient Implementation of Weighted ENO Schemes," J. Comput. Phys., Vol. 126, 1996, pp. 202-228.

Kang, S., Iaccarino, G., Ham, F. and Moin P., "Prediction of Wall-Pressure Fluctuation in Turbulent Flows with an Immersed Boundary Method," J. Comput. Phys., Vol. 228, 2009, pp. 6753-6772.

Kalitzin, G., Medic, G., Iaccarino, G. and Durbin, P., "Near-Wall Behavior of RANS Turbulence Models and Implications for Wall Functions," J. Comput. Phys., Vol. 204, 2005, pp. 265-291.

Kim, D. and Choi, H., "Immersed Boundary Method for Flow around an Arbitrary Moving Body," J. Comput. Phys., Vol. 212, 2006, pp. 662-680.

Leonard, B.P., "Stable and Accurate Convective Modeling Procedure Based on Quadratic Upstream Interpolation," Comput. Meth. Appl. Mech. Eng., Vol. 19, 1979, pp. 59-98.

Meneveau, C., Lund, C.S., and Cabot, W.H., "A Lagrangian Dynamic Subgrid-scale Model of Turbulence," J. Fluid Mech., Vol. 319, 1996, pp. 353-385.

Menter, F. R., "Two-Equation Eddy Viscosity Turbulence Models for Engineering Applications," AIAA J., Vol.32, 1994, pp.1598-1605.

Noack, R.W., "SUGGAR: a General Capability for Moving Body Overset Grid Assembly," 17th AIAA Computational Fluid Dynamics Conference, Toronto, Ontario, Canada, 2006.

Sethian, J. A., "A Fast Marching Level Set Method for Monotonically Advancing Fronts," Proc. Natl. Acad. Sci. USA, Vo. 93, 1996 pp. 1591-1595.

Spalart, P. R. and Allmaras, S. R., 1992, "A One-Equation Turbulence Model for Aerodynamic Flows," AIAA Paper 92-0439.

Suh, J., Yang, J. and Stern, F., "The Effect of Air-Water Interface on the Vortex Shedding from a Vertical Circular Cylinder," J. Fluids Struct., 2010, under revision.

Sussman, M., Smereka, P. and Osher, S., "A Level Set Approach for Computing Solutions to Incompressible Two-Phase Flow," J. Comp. Phys., Vol. 114, 1994, pp. 146-159.

Wang, Z., Yang, J. and Stern F. F. Stern, "An Improved Particle Correction Procedure for the Particle Level Set Method," J. Comput. Phys., Vol. 228, 2009a, pp. 5819-5837.

Wang, Z., Yang, J., Koo, B. and Stern F. F. Stern, "A Coupled Level Set and Volume-of-Fluid Method for Sharp Interface Simulation of Plunging Breaking Waves," Inter. J. Multiphase Flow, Vol. 35, 2009b, pp. 227-246.

Xu, S., "The Immersed Interface Method for Simulating Prescribed Motion of Rigid Objects in an Incompressible Viscous Flow," J. Comput. Phys., Vol. 227, 2008, pp.5045-5071.

Yang, J. and Balaras, E., "An Embedded-Boundary Formulation for Large-Eddy Simulation of Turbulent Flows Interacting with Moving Boundaries," J. Comput. Phys., Vol. 215, 2006, pp. 12-40.

Yang, J., Sakamoto, N., Wang, Z., Carrica, P.M. and Stern, F., "Two Phase Level-Set/Immersed-Boundary Cartesian Grid Method for Ship Hydrodynamics," Proc. 9th Inter. Conf. Numer. Ship Hydrodynamics, Ann Arbor, Michigan, 2007.

Yang, J., Preidikman, S., and Balaras, E., A strongly-coupled, embedded-boundary method for fluid-structure interactions of elastically mounted rigid bodies, J. Fluids Struct., Vol. 24, 2008a, pp. 167-182.

Yang, J., Bhushan, S., Suh, J., Wang, Z., Koo, B., Sakamoto, N., Xing, T. and Stern, F., "Large-eddy simulation of ship flows with wall-layer models on Cartesian grids," 27th Symposium on Naval Hydrodynamics, Seoul, Korea, 2008b.

Yang, J. and Stern, F., "Sharp Interface Immersed-Boundary/Level-Set Method for Wave-Body Interactions," J. Comput. Phys., Vol. 228, 2009, pp. 6590-6616.

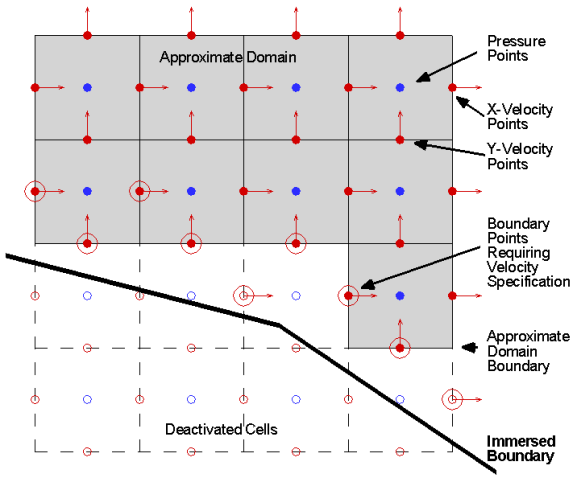

Figure 1: Approximate domain on staggered grid.

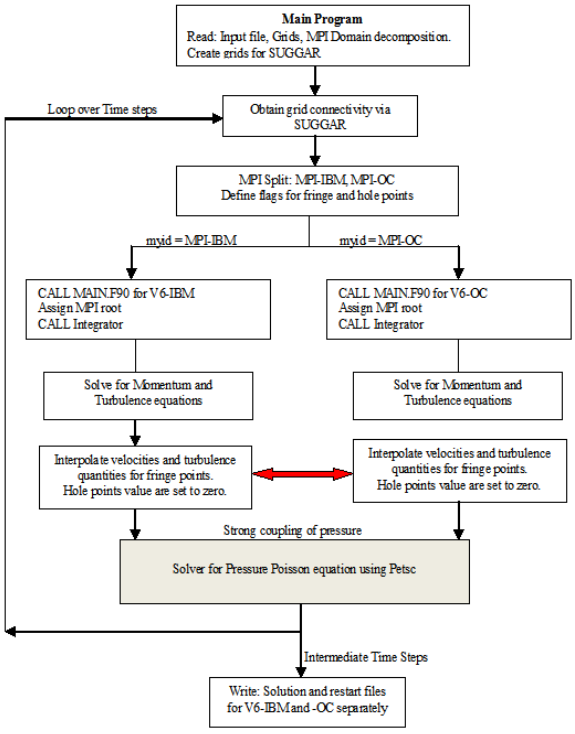

Figure 2. Flow chart demonstrating steps involved in coupling V6-IBM and V6-OC solvers.

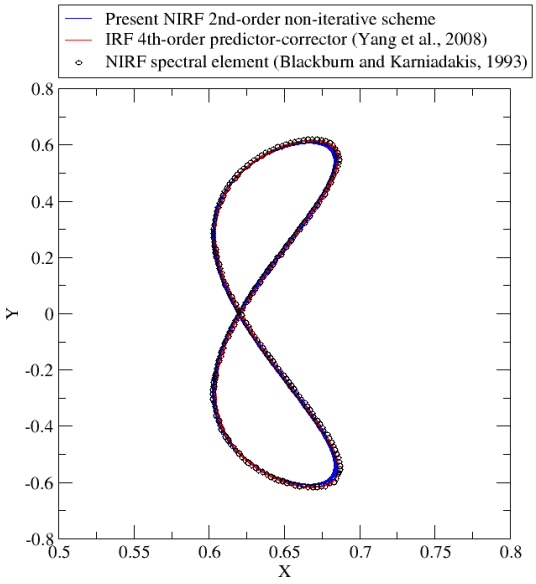

Figure 3. Centerline displacement phase plot with reference data for a circular cylinder freely vibrating in the (x; y) plane in a free stream.

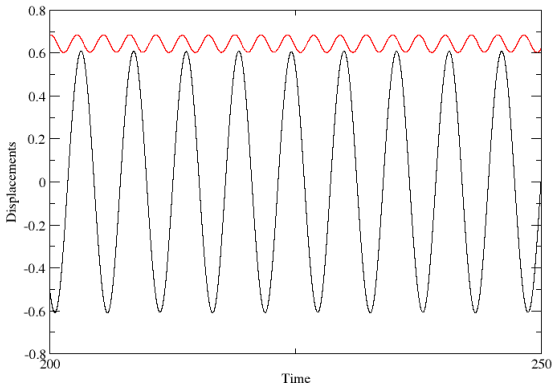

Figure 4. Time history of displacements in x and y directions for a circular cylinder freely vibrating in the (x; y) plane in a free stream.

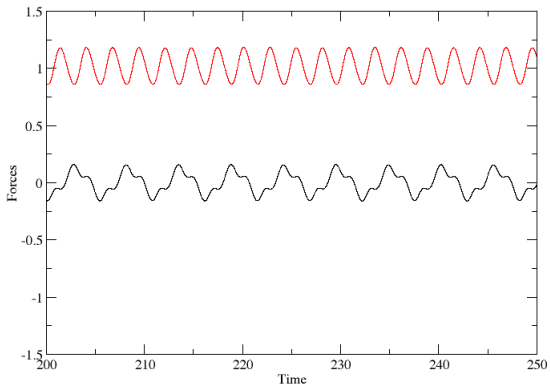

Figure 5. Time history of hydrodynamic forces in x and y directions for a circular cylinder freely vibrating in the (x; y) plane in a free stream.

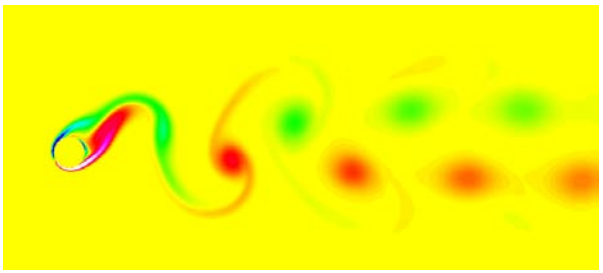

Figure 6. A snapshot of vorticity contours for a circular cylinder freely vibrating in the (x; y) plane in a free stream.

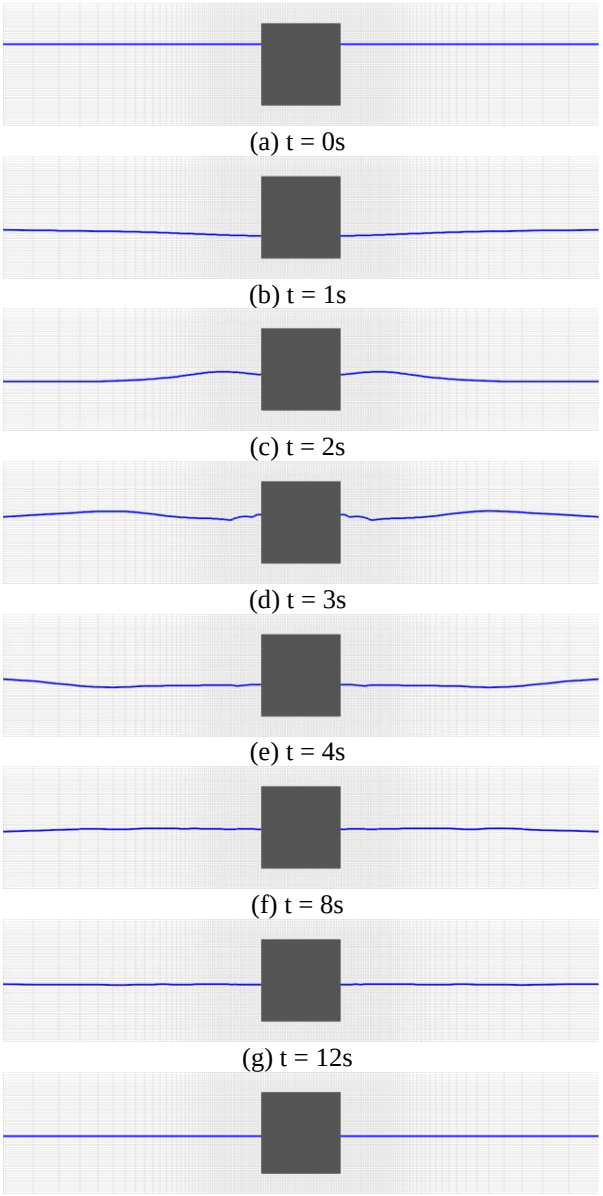

(a) t = 0s

(b) t = 1s

(c) t = 2s

(d) t = 3s

(e) t = 4s

(f) t = 8s

(g) t = 12s

(h) t = 100s

Figure 7. Snapshots of interface profile for a half-buoyant square cylinder reaching equilibrium state.

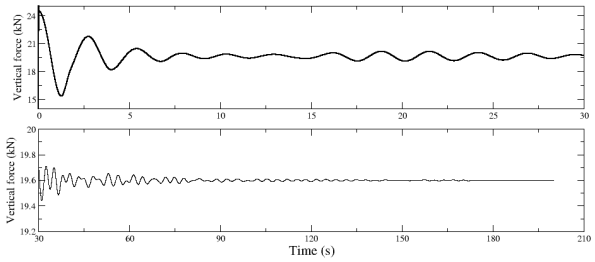

Figure 8. Time history of vertical hydrodynamic force on a half-buoyant square cylinder reaching equilibrium state.

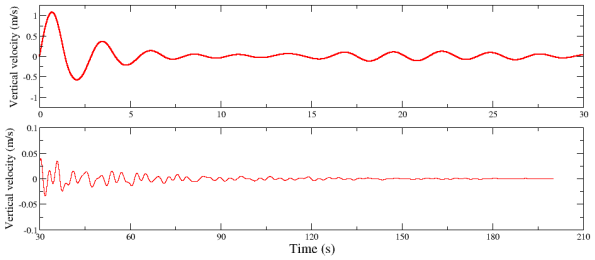

Figure 9. Time history of vertical velocity of a half-buoyant square cylinder reaching equilibrium state.

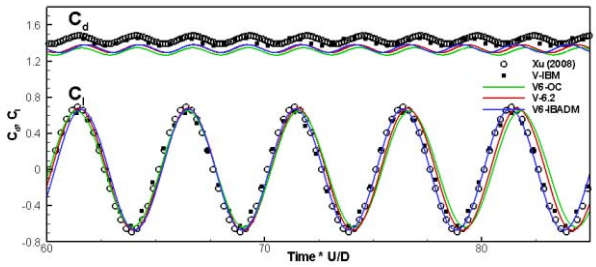

Figure 10. Comparison of CFDShip-Iowa version 6 results with data from Xu (2008) for 2D circular cylinder at Re = 200.

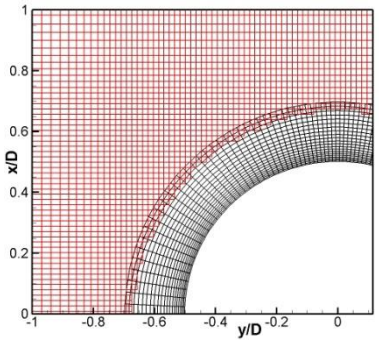

(a)

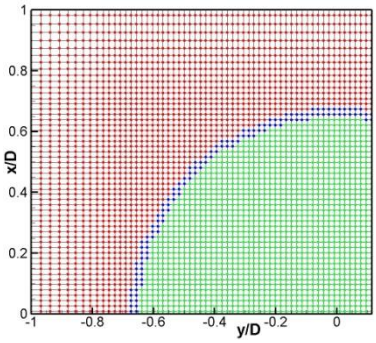

(b)

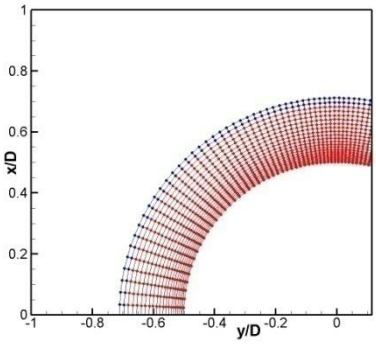

(c)

Figure 11. (a) Overset grid configuration for a circular cylinder, (b) fluid points (RED), fringe points (BLUE) and hole points (GREEN) are shown for the Cartesian grid, and (c) fringe and fluid points are shown for the wall-layer grid.

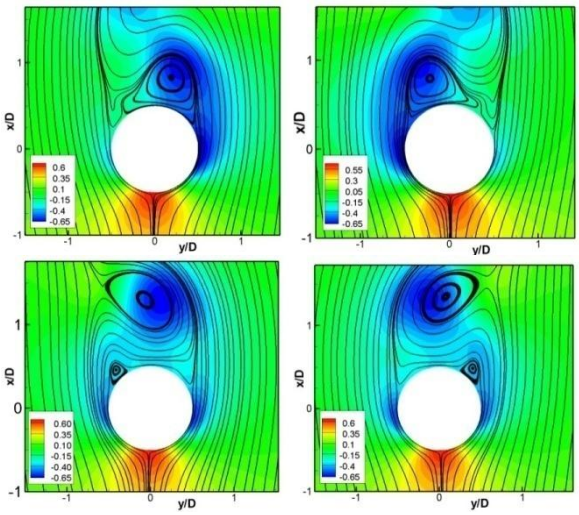

Figure 12. Quarter phases of vortex shedding obtained using V6.2 for Re = 200. Pressure contours are shown.

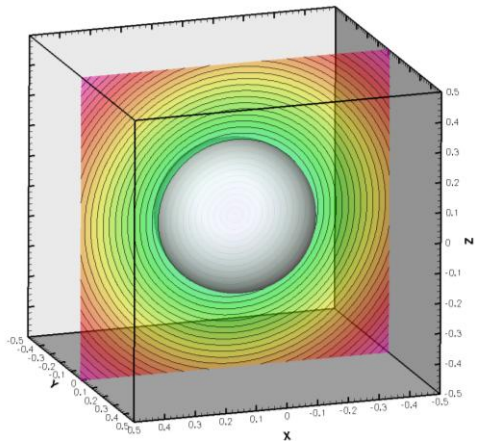

Figure 13. A test case for the signed distance function calculation using a parallel fast marching method.

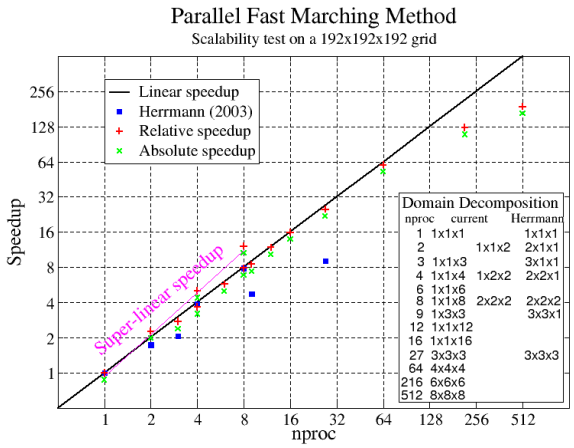

Figure 14. Parallel speedup of the current parallel fast marching method in a simple test case.

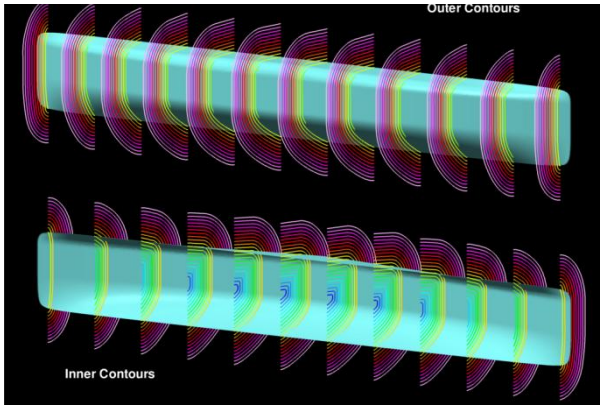

Figure 15. Signed distance function for Wigley hull.

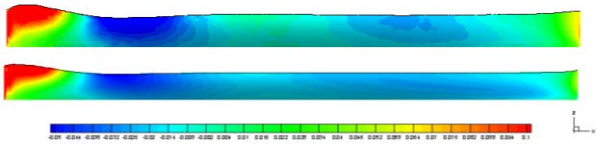

Figure 16: Predicted pressure distribution on hull surface with IBM (top) compared with body-fitted solver (bottom) (Huang et al., 2007).

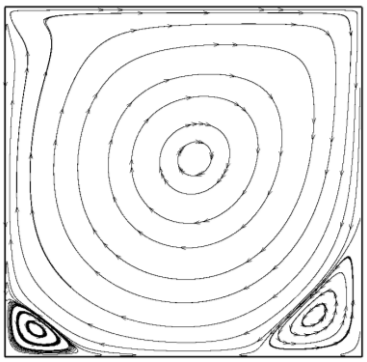

(a)

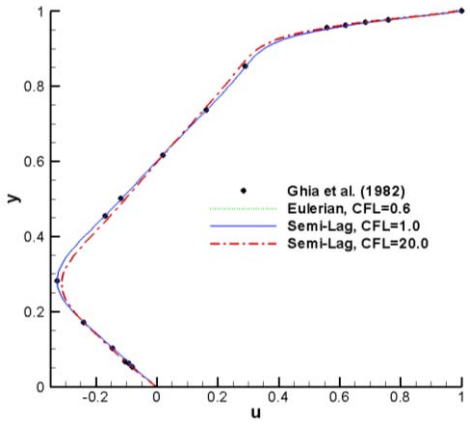

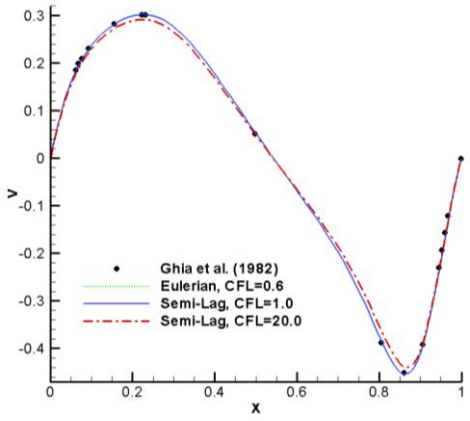

Figure.17. Lid-driven cavity flow at Re=400 on a 100×100 grid. Left: streamlines; center: profile of the horizontal velocity component along the vertical centerline; right: profile of the vertical velocity component along the horizontal centerline.

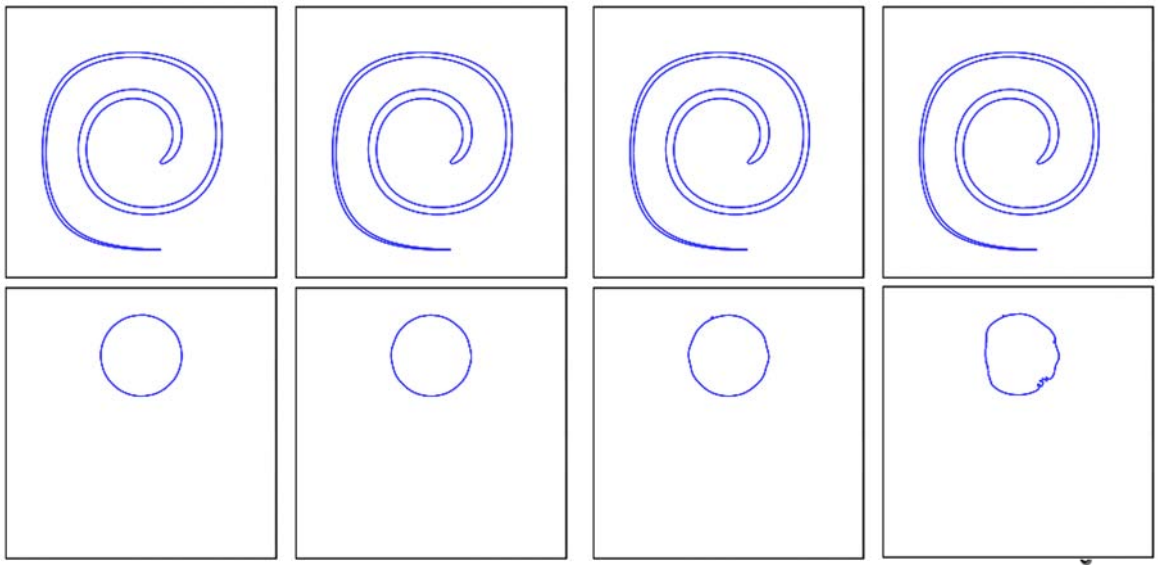

(a) (b) (c) (d)

Figure 18. Single vortex flow advection test on a 512×512 grid. (a): Eulerian, CFL=0.32; (b) Semi-Lagrangian, CFL=1.0; (c) semi-Lagrangian, CFL=2.0; (d) Semi-Lagrangian, CFL=3.0.

Table 1: Grids, drag and lift coefficients, and Strouhal number for flow past circular cylinder, Re = 200.

	WL domain	**Grid resolution**		**C_d**		**C_l**		**S_t**
		$N_x \times N_y$	$N_r \times N_\theta$	Mean	Amplitude	Mean	Amplitude	
Xu (2008)	-	-	-	1.44	0.045	0	0.68	0.201
Averaged CFD (Xu, 2008)	-	-	-	1.40	0.042	0	0.64	0.200
V6-IBM	-	204×260	-	1.41	0.040	0	0.64	0.200
V6-IBADM		180×244		1.34	0.043	0	0.67	0.203
V6.2	$0.2D_o$	204×260	22×128	1.34	0.043	0	0.67	0.199